ROYAL SOCIETY OF CHEMISTRY

PAPER

Check for updates

Structure–property relationship study of blue thermally activated delayed fluorescence molecules with different donor and position substitutions: theoretical perspective and molecular design†

Yuzhi Song,* Bihe Li, Songsong Liu, Ming Qin, Yang Gao, Kai Zhang, [iD] Lili Lin, [iD] Chuan-Kui Wang and Jianzhong Fan [iD] *

Blue-efficient thermally-activated delayed fluorescence emitters are widely desired in organic light-emitting diodes due to their advantages in both improving display resolution and providing better pixels. However, both the species and amounts of blue-TADF molecules are far from meeting the requirement for practical applications. Thus, systematic studies are desired to study the relationship between molecular structures and luminescent properties. Herein, a total of 15 molecules with different donor substitutions (DMAC, PXZ, PTZ, DPA and Cz) and different position substitutions (*ortho*, *meta* and *para*) are designed and their photophysical properties are studied in detail utilizing density functional theory (DFT) and time-dependent DFT methods. The conformational isomerization, intramolecular interactions, energy gaps, spin–orbit couplings, and fluorescence efficiencies are analyzed. Moreover, the radiative and non-radiative as well as the intersystem crossing (ISC) and reverse intersystem crossing (RISC) processes are investigated using the thermal vibration correlation function method. Results indicate that molecules with *m*-substitutions possess the largest energy gap between the lowest singlet and triplet excited states. However, molecules with DPA and Cz substitutions can bring remarkable spin–orbit coupling effects, excellent radiative decay rate and efficient ISC and RISC rates. By analyzing the calculated quantum efficiencies, five promising blue-TADF molecules (*o*-DPA-QL, *m*-DPA-QL, *p*-DPA-QL, *o*-Cz-QL and *m*-Cz-QL) with stable nearly planar conformations are theoretically proposed. Our work gives reasonable explanations for experimental measurements and provides a molecular design strategy for efficient blue-TADF molecules.

1. Introduction

Recently, organic light-emitting diodes (OLEDs) have shown promising applications in new-generation organic lighting and flexible displays. According to multiplicities of angular momentum and spin properties randomly, only 25% of the injected charges are used in conventional fluorescent OLEDs. For solving this problem, phosphorescent devices were proposed. However, the annihilation effect of triplet states at high current densities is particularly serious for phosphorescent devices, leading to severe device efficiency degradation. In order to avoid this adverse effect,

triplet–triplet annihilation (TTA), hybridized local and charge transfer (HLCT), and thermally activated delayed fluorescence (TADF) materials have emerged generationally. TADF materials possess the advantages of low-cost and stable features, and are most rapidly developing amongst the TTA, HLCT and TADF materials. In 2009, Adachi and colleagues made the first attempt to apply TADF in OLEDs.[1] Later, tremendous endeavors have been devoted to developing highly efficient TADF emitters with panchromatic emissions. For example, Adachi and colleagues made significant progress in 2012 with external quantum efficiency (EQE) of 19.3% in the TADF OLED.[2] Tang *et al.* found that the TADF properties of a compound can be systematically tuned *via* its aggregation state to realize multifunctional emitting materials.[3] Moreover, they transformed 2,3,4,5,6-penta (9*H*-carbazol-9-yl) benzonitrile from an aggregation-caused quenching molecule into an aggregation-induced emission (AIEgen), which gives an approach to explore efficient emitters

Shandong Province Key Laboratory of Medical Physics and Image Processing Technology, Institute of Materials and Clean Energy, School of Physics and Electronics, Shandong Normal University, 250014 Jinan, China.
E-mail: fanjianzhongvip@163.com, yzsong@sdnu.edu.cn

This journal is © The Royal Society of Chemistry 2022

J. Mater. Chem. C, 2022, **10**, 4723–4736 | **4723**

by combining AIE with TADF.[4] Ma *et al.* found that the molar extinction coefficients and photoluminescence quantum yields (PLQYs) of the two dual emitting cores (2,2′-DPXZ-PN and 3,3′-DPXZ-PN) were also significantly improved.[5] Xu *et al.* constructed dual-doped white TADF films and achieved white color purity with a high quantum yield of ∼90%.[6] Chi *et al.* found that the TADF emitters (PCz and PSz) with shorter *p*-linkers exhibit high PLQYs(50.81% and 59.15%) and device performance with EQEs ranged from 20% to 30%.[7] Yang's group found that OLEDs using *o*B-2Cz and *o*B-2tCz as emissive guests can reach their maximum EQEs of 28.1% and 27.5%, respectively.[8] Li *et al.* synthesized three molecules 3Cz-Ph-CN, 3Cz-mPh-CN and 3Ph-Cz-CN, which achieved high external quantum efficiency of 18.1%.[9] Duan *et al.* obtained a high reverse intersystem crossing rate (K_{RISC}) of 2.36×10^6 s^{-1} with an emission peak of 456 nm and maximum EQE of 22.8% by replacing the stronger cyano acceptor with the weak acceptor of cyanophenyl.[10] In addition, many efforts have been devoted to develop efficient TADF materials.[11–23] Currently, green and red TADF materials have achieved high efficiency and good device stability.[24–28] However, due to the wide band gap required for blue materials, the efficiency and lifetime are unsatisfactory to achieve available application.[29–31] Thus, highly efficient blue TADF materials are a highly desired.[32] To achieve efficient delayed fluorescence emission, the usually adopted strategy is building highly twisted D–A typed molecules with intramolecular charge transfer (ICT) feature, which well separates the distributions of highest occupied molecular (HOMO) and lowest unoccupied molecular orbital (LUMO). This steric hindrance effect facilitates intramolecular twisting and reduces the energy gap (ΔE_{ST}) between the lowest singlet (S$_1$) and triplet (T$_1$) excited states. Following the equations of $\Delta E_{ST} = E_S - E_T = 2J$, $J = \iint \Phi_L(1)\Phi_H(2)\dfrac{e^2}{r_1 - r_2}\Phi_L(2)\Phi_H(1)dr_1dr_2$ and $\mu = \iint \Phi_L(1)\Phi_H(2)r_{12}\Phi_L(2)\Phi_H(1)dr_1dr_2$, J is the exchange energy of the two unpaired electrons at the excited states and μ represents the transition dipole moment. E_s and E_t are adiabatic singlet and triplet energies, respectively. Theoretical investigations show that the increase in the density of HOMO–LUMO overlap leads to an increase in the transition dipole moment and luminescence efficiency.[33] Therefore, the synergistic effect between ΔE_{ST} and PLQY generated by the appropriate construction of the donor and acceptor is important. The relationship between high exciton utilization and high efficiency needs to be carefully balanced.

Recently, Chen *et al.* reported three quinoline-based TADF molecules, namely 9,9-dimethyl-10-(quinolin-2-yl)-9, 10-dihydroacridine (DMAC-QL), 10-(quinolin-2-yl)-10*H*-phenoxazine (PXZ-QL) and 10-(quinolin-2-yl)-10*H*-phenothiazine (PTZ-QL).[34] The twisted conformations were confirmed and all the compounds exhibit high thermal stability. The ΔE_{ST} values of DMAC-QL, PXZ-QL and PTZ-QL are 0.06, 0.10 and 0.04 eV, respectively, which means that they may have excellent TADF properties. The non-doped OLEDs based on the three emitters were manufactured, the maximal EQEs of the devices achieved 7.7, 17.3 and 14.8%, respectively. As we know, donors with more than one conformation (such as

DMAC, PXZ and PTZ) have negative repercussions in TADF OLEDs.[35] In order to better illustrate the relationship between molecular structures and luminescent properties and improve the efficiency of these TADF molecules, we are motivated to investigate the TADF properties of total of 15 molecules with QL as an acceptor, DMAC, PXZ, PTZ, DPA and Cz as donors, as well as different position substitutions (ortho, meta and para) by using density functional theory (DFT) and time-dependent DFT (TD-DFT) methods applied using GAUSSIAN 16.[36,37] By analyzing the energy gaps, intramolecular interactions and non-radiative decay rates as well as intersystem crossing (ISC) and reverse intersystem crossing (RISC) rates, experimental measurements are reasonably explained and five promising blue-TADF molecules (*o*-DPA-QL, *m*-DPA-QL, *p*-DPA-QL, *o*-Cz-QL and *m*-Cz-QL) are theoretically proposed.

2. The theoretical method

By employing the polarizable continuum model (PCM)[38,39] to consider the solution effect of tetrahydrofuran (THF), the properties of the ground and excited states for 15 TADF molecules (shown in Fig. 1) are theoretically studied by DFT and TD-DFT, respectively.[40] By comparing the emission wavelengths calculated using different functionals of O3LYP,[41] B3LYP,[42] PBE0,[43] M062x[44] and BMK,[44] the PBE0 coupled with 6-31G* basis set was determined. The correspondingly calculated data and experimental results are shown in Table 1. The geometries of the ground and excited states are fully optimized and no imaginary frequencies are found, which confirms the stable structures. Furthermore, the radiative decay rate from S$_1$ to ground state (S$_0$) was calculated using the following equation:

$$K_r = \int \delta_{em}(\omega, T)d\omega, \tag{1}$$

where the emission spectrum $\delta_{em}(\omega,T)$ can be expressed as

$$\delta_{em}(\omega, T) = \frac{4\omega^3}{3\hbar c^3}\sum_{\mu,\nu} P_{i\nu}\left|\left\langle \Theta_{f\mu}|\mu_{fi}|\Theta_{i\nu}\right\rangle\right|^2 \delta(\omega_{i\nu,f\mu} - \omega) \tag{2}$$

Here, $\mu_{fi} = \langle \theta_f|\bar{\mu}|\theta_i\rangle$ is the electric transition dipole moment between the two electronic states, $P_{i\nu}$ represents the Boltzmann distribution function.

As for the non-radiative decay rate, it can be estimated under Fermi's gold rule by equation:

$$K_{nr} = \frac{2\pi}{\hbar}\sum_{kl} R_{kl}Z_i^{-1}\sum_{vu} e^{-\beta E_{iv}}\left\langle \Theta_{fu}|\hat{P}_{fk}|\Theta_{iv}\right\rangle$$
$$\times \left\langle \Theta_{iv}|\hat{P}_{fl}|\Theta_{fu}\right\rangle \delta(E_{iv} - E_{fu}) \tag{3}$$

Where, $R_{kl} = \langle \Phi_f|\hat{P}_{fk}|\Phi_i\rangle\langle\Phi_i|\hat{P}_{fl}|\Phi_f\rangle$ is a non-adiabatic electron coupling term. $\hat{P}_{fk} = -i\hbar\dfrac{\partial}{\partial Q_{fk}}$ represents the normal momentum operator of the *k*th normal mode in the final electronic state. Further, through the Fourier transform of the incremental

4724 | *J. Mater. Chem. C*, 2022, **10**, 4723–4736

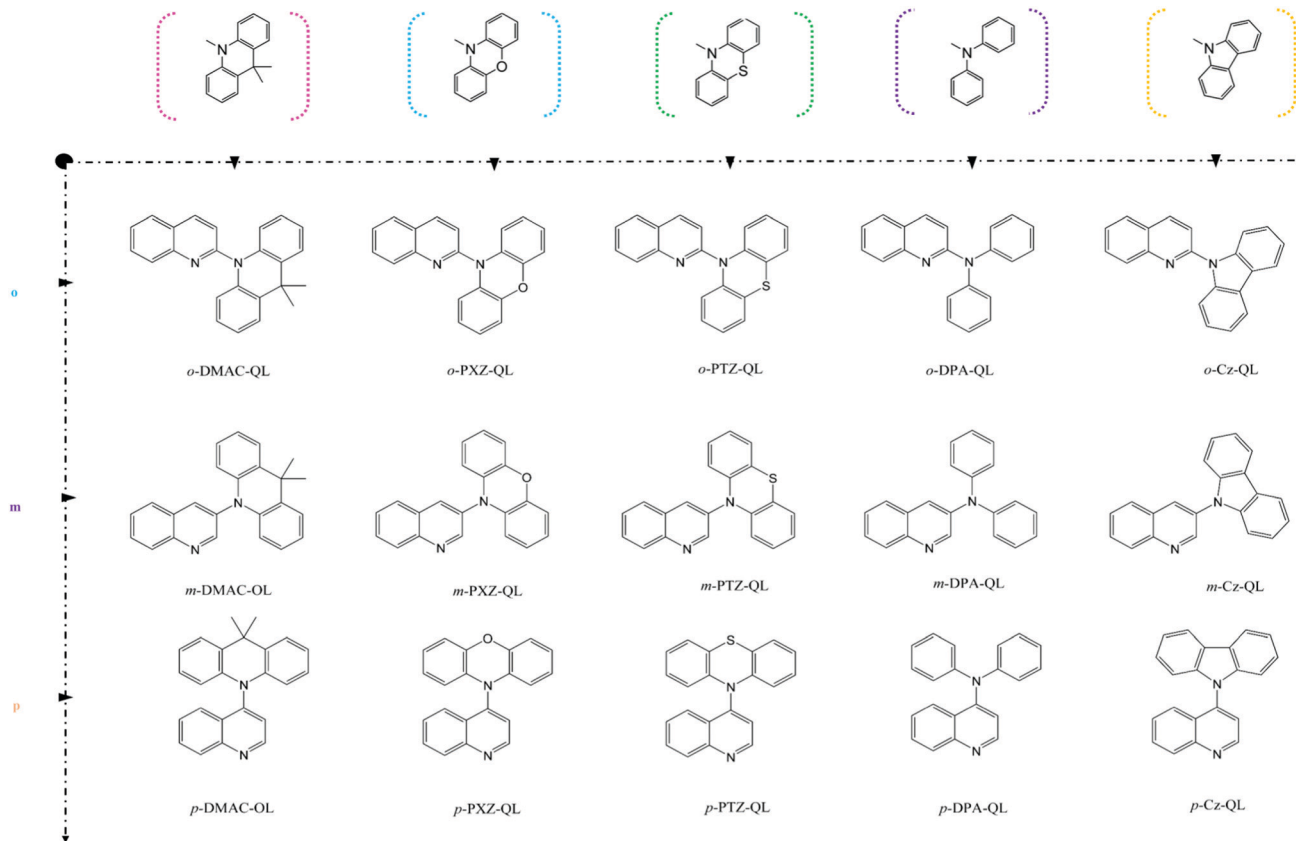This journal is © The Royal Society of Chemistry 2022

Fig. 1 Molecular structures of all studied molecules.

Table 1 The calculated emission wavelengths with different functionals and the corresponding experimental data

	HF (%)	DMAC-QL (nm)	PXZ-QL (nm)	PTZ-QL (nm)
O3LYP	11.61	619.73	750.94	739.20
B3LYP	20	545.96	640.09	629.06
PBE0	25	506.24	587.76	571.31
BMK	42	427.05	483.78	464.55
M062x	54	391.85	433.51	430.28
Exp.		511.00	554.00	561.00

function, the formula can be expressed as follows:

$$K_{nr} = \sum_{kl} \frac{1}{\hbar^2} R_{kl} \int_{-\infty}^{\infty} dt \left[e^{i\omega_{if}t} Z_i^{-1} \rho_{ic,kl}(t,T) \right] \quad (4)$$

Z_i is the partition function. $\rho_{ic,kl}(t,T) = \mathrm{Tr}(\hat{P}_{fk} e^{-i\tau_f \hat{H}_f} \hat{P}_{fl} e^{-i\tau_i \hat{H}_i})$ is the thermal vibration correlation function (TVCF).

The ISC and RISC rates for TADF systems can be expressed as:[45]

$$K_{ISC} = \frac{1}{\hbar^2} \langle \Phi_f | \hat{H}^{SO} | \Phi_i \rangle \int_{-\infty}^{\infty} dt \left[e^{i\omega_{if}t} Z_i^{-1} \rho_{ISC}(t,T) \right] \quad (5)$$

Here, $\langle \Phi_f | \hat{H}^{SO} | \Phi_i \rangle$ is the spin–orbit coupling (SOC) coefficient between two states, which can be quantitatively calculated by Dalton 2013.[46,47]

According to these rates, the PL quantum efficiencies can be calculated by the following:

$$\Phi_{PF} = \frac{K_r^S}{K_r^S + K_{nr}^S + K_{ISC}} \quad (6)$$

$$\Phi_{DF} = \sum_{k=1}^{\infty} (\Phi_{ISC}\Phi_{RISC})^k \Phi_{PF} = \frac{\Phi_{ISC}\Phi_{RISC}}{1 - \Phi_{ISC}\Phi_{RISC}} \Phi_{PF} \quad (7)$$

Where, Φ_{ISC} and Φ_{RISC} represent the intersystem crossing efficiency and reverse intersystem crossing efficiency, respectively, which can be written as the following:

$$\Phi_{ISC} = \frac{K_{ISC}}{K_r^S + K_{nr}^S + K_{ISC}} \quad (8)$$

$$\Phi_{RISC} = \frac{K_{RISC}}{K_r^T + K_{nr}^T + K_{RISC}} \quad (9)$$

All these decay rates can be obtained by using the MOMAP software package.[48] Both, the detailed methodology and simulation method of the above formalism can be found in the works of Peng, Shuai and us.[49–55] In addition, the frontier molecular orbitals, intramolecular interactions and natural transition orbit (NTO) analyses were performed following Multiwfn.[56]

This journal is © The Royal Society of Chemistry 2022

J. Mater. Chem. C, 2022, **10**, 4723–4736 | **4725**

3. Results and discussions

Based on the research of Chen's group, the reported 3 molecules (o-DMAC-QL, o-PXZ-QL and o-PTZ-QL) were selected and investigated. Moreover, 12 new molecules with different donor and position substitutions were theoretically designed and studied (m-DMAC-QL, p-DMAC-QL, m-PXZ-QL, p-PXZ-QL, m-PTZ-QL, p-PTZ-QL, o-DPA-QL, m-DPA-QL, p-DPA-QL, o-Cz-QL, m-Cz-QL and p-Cz-QL). Thus, the photophysical properties of total of 15 molecules are studied in detail. In order to design and select efficient blue-TADF molecules, we divided 15 molecules into 5 groups by different donor substitutions (DMAC, PXZ, PTZ, DPA and Cz). While, they were divided into 3 groups by different position substitutions (ortho, meta, and para). Results show that, for molecules with different positional substitutions, the order of probabilities of nearly orthogonal conformations is o-substitutions < m-substitutions < p-substitutions. For molecules with DPA and Cz substitutions, they have larger SOC values, considerable radiative decay rate (K_r) and ISC/RISC rates than the molecules with DMAC, PXZ and PTZ substitutions. Finally, five promising blue-TADF molecules were determined (o-DPA-QL, m-DPA-QL, p-DPA-QL, o-Cz-QL and m-Cz-QL). Detailed analyses are discussed in the following sections.

3.1 Conformational isomerization

The focus for the design of TADF molecules was based upon a single equilibrium picture until recently. However, the presence of some conformations may cause an effective loss pathway photophysically. So, it is necessary to analyze the ratio of multiple conformations in the design of TADF molecules.

According to recent reports, molecules constructed from pseudoplanar segments (DMAC, PTZ, PXZ and DMDB) may have dual conformations (nearly planar conformation and nearly orthogonal conformation).[57,58] To better illustrate this issue further, the potential energy curves (PECs) of total molecules were studied and are displayed in Fig. 2. Results show that some of the molecules with DMAC, PTZ and PXZ substitutions possess dual conformations indeed, which is consistent with the previously reported work.[59,60] Meanwhile, the molecules with DPA and Cz substitutions only possess single conformations.

As for DMAC, PXZ and PTZ with dual conformations, the situation is complex. As proposed by Boltzmann et al.,[35] the relative ratios for multiple conformations (such as DMAC, PXZ and PTZ) can be calculated by the following equation:

$$\% \, \text{conformer}_i = \frac{\exp\left(-\dfrac{E_i}{k_b T}\right)}{\sum_j \exp\left(-\dfrac{E_j}{k_b T}\right)} \tag{10}$$

Where k_b is the Boltzmann constant, E is the conformational relative energy and T is the environmental temperature. For molecules with o-substitutions, the energy of nearly planar conformation is lower than that of the nearly orthogonal conformation for o-DMAC-QL (Fig. 2a), even though there are only nearly planar conformations such as o-PXZ-QL (Fig. 2d) and o-PTZ-QL (Fig. 2g). Following eqn (10), the probabilities of

nearly orthogonal conformations are very small for molecules with o-substitutions. For molecules with m-substitutions and p-substitutions, the energies of nearly orthogonal conformations are lower than nearly planar conformations (Fig. 2b, c and 2h, i), even though there are only nearly orthogonal conformations (Fig. 2e and f). Meanwhile, for molecules with p-substitutions, the energy gaps between nearly planar conformations and nearly orthogonal conformations are larger than those for m-substitutions. Therefore, the probabilities of nearly orthogonal conformations for molecules with p-substitutions are higher than molecules with m-substitutions. In conclusion, for molecules with dual conformations, the probabilities of nearly orthogonal conformations are in the order of o-substitutions < m-substitutions < p-substitutions.

As for DPA and Cz with a single conformation, the order that two valleys of PECs approaching 90° is: o-substitutions < m-substitutions < p-substitutions (Fig. 2j–o). Consequently, for molecules with single conformations, the probabilities of the nearly orthogonal conformations are in the order of o-substitutions < m-substitutions < p-substitutions.

Considering the above two conditions, the probabilities of nearly orthogonal confirmation for studied molecules can be roughly estimated, the order is o-substitutions < m-substitutions < p-substitutions. The analyses of conformational isomerization facilitate screening of the blue-TADF molecules with the highest probabilities of being present.

3.2 The molecular geometries

Previous theoretical calculations indicate that the distance between the donor and the acceptor plays a key factor in PLQY and EQE.[61] Following the reported result by Lu, the chemiluminescence resonance energy transfer efficiency is inversely proportional to the sixth power of the donor–acceptor distance, which is consistent with Förster's resonance theory.[62] The twist angle and rotation motion between the donor and acceptor in D–A typed molecules play an important role in the photophysical properties of such molecules.[63] Based on optimized structure (S_0), the bond length and dihedral angle between D–A typed groups are obtained and shown in Table 2. By analyzing the data, it can be found that the bond lengths and the dihedral angles between D–A typed groups are both in order of o-substitutions < m-substitutions < p-substitutions. Thus, the order of molecular geometries that approach orthogonality is: o-substitutions < m-substitutions < p-substitutions.

The orthogonality of molecular geometries may influence the overlap between HOMO and LUMO, which are shown in Fig. S6 (ESI†) and the detailed data are listed in Table S1 (ESI†). Results indicate that the substitution effects of o-positions and m-positions may give a larger overlap between HOMO and LUMO than p-positions. Furthermore, a large overlap between HOMO and LUMO may promote the radiative process.[33]

Thus, the findings described in this section were verified from those in the last section by connecting the bond length and dihedral angle. In addition, for molecules with DPA and Cz substitutions, substitution effects of o-positions and m-positions
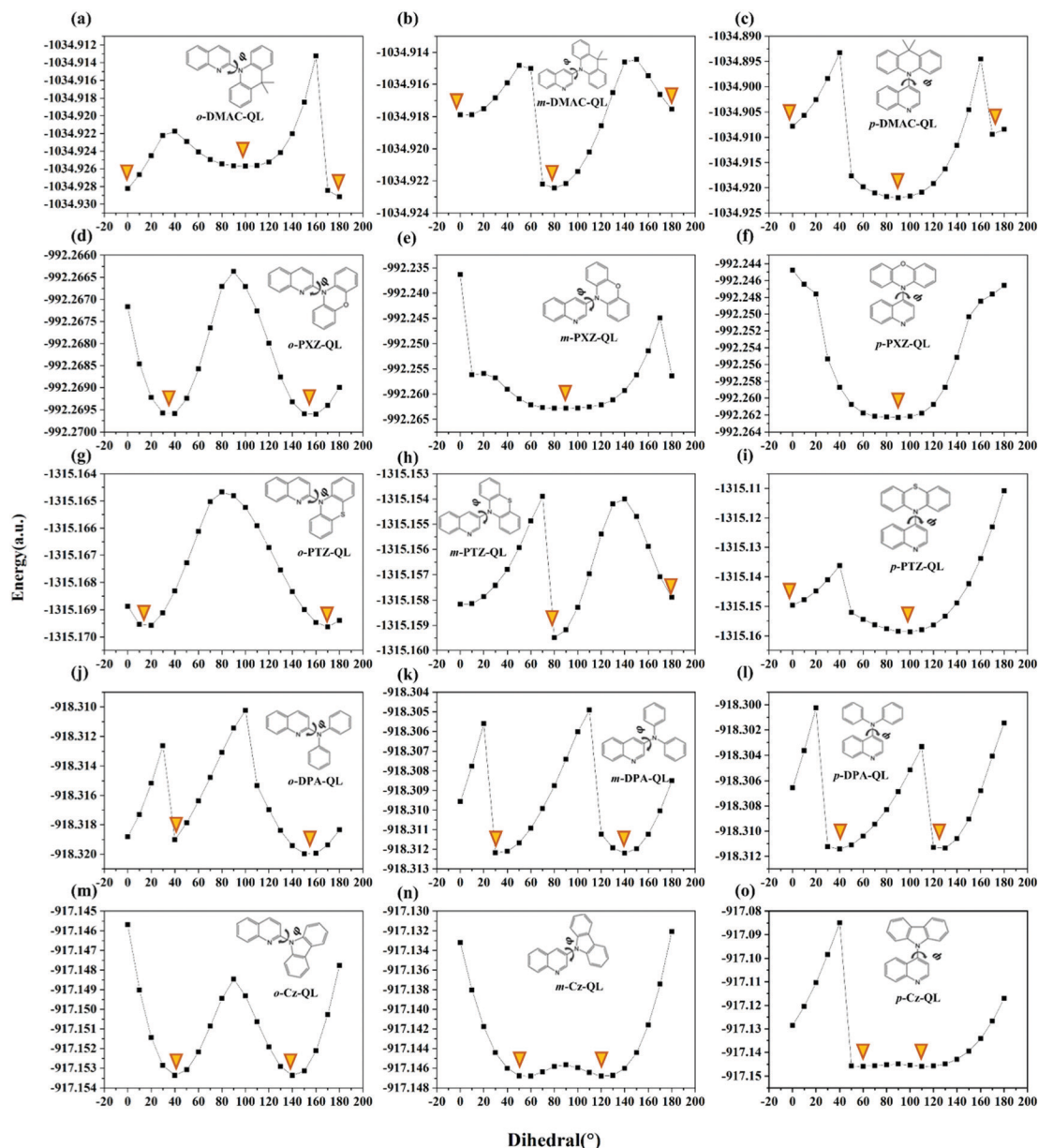
Fig. 2 Potential energy curves of ground states of a total of 15 studied molecules in tetrahydrofuran. φ represents the dihedral angle between D and A fragments, which is marked with a rotating arrow. Orange inverted triangle represents the valley.

may promote the radiative process. More evidence is provided in the following sections.

3.3 Intramolecular interactions and energy gaps

As we know, the photophysical properties are largely affected by the intramolecular interactions, the weak intramolecular interactions are identified by reduced density gradient (RDG) analyses embedded in the Multiwfn software.[64] The corresponding results for a total of 15 molecules are shown in Fig. 3 and Fig. S1 and S2 (ESI†). It confirmed that there is a weak van der Waals (green isosurface) interaction between the C–H bonds of donor and acceptor. We find that the D and A fragments had red fusiform areas in the middle of the benzene ring, so it also confirms that the D and A fragments have a

strong steric hindrance (red isosurface). For molecules with different positional substitutions, the intramolecular interactions have a weak effect on molecules with o-DMAC-QL (Fig. S1a, ESI†), o-PXZ-QL (Fig. 3a) and o-PTZ-QL (Fig. S2a, ESI†). Because these molecules possess nearly planar conformations, the intramolecular interactions (attraction) are obviously influenced by the closer distance between the N of the acceptor and H of the donor. For the molecules with DPA (Fig. S2d–S2f, ESI†) and Cz (Fig. 3d–f) substitutions, the attraction of intramolecular interactions becomes weaker than the molecules with DMAC, PXZ and PTZ substitutions because the electron-donating abilities of DPA and Cz are weaker than DMAC, PXZ and PTZ, which is good for constructing blue-TADF molecules.

Table 2 Collected bond lengths and dihedral angles between the donor and acceptor groups for all the studied molecules in the ground state (S_0)

System	Bond length/Å	Dihedral angle/°
o-DMAC-QL	1.398	22.91
m-DMAC-QL	1.422	88.45
p-DMAC-QL	1.424	90.09
o-PXZ-QL	1.402	35.21
m-PXZ-QL	1.420	84.42
p-PXZ-QL	1.421	89.82
o-PTZ-QL	1.398	15.60
m-PTZ-QL	1.427	79.88
p-PTZ-QL	1.429	97.41
o-DPA-QL	1.395	60.03
m-DPA-QL	1.403	67.10
p-DPA-QL	1.406	76.03
o-Cz-QL	1.406	41.13
m-Cz-QL	1.408	55.31
p-Cz-QL	1.411	57.94

Furthermore, ΔE_{ST} is an important factor to determine the RISC process of TADF molecules.[65,66] The adiabatic excitation energies are shown in Fig. 4, and the detailed data are collected in Table 3. According to recently reported work, the large energy

gap between S_1 and S_0 is beneficial for blue-TADF molecules.[67] As for the molecules with DPA and Cz substitutions, the energy gaps between S_1 and S_0 (2.94–3.30 eV) are higher than the molecules with DMAC (2.63–2.75 eV), PXZ (2.32–2.40 eV) and PTZ (2.43–2.50 eV) substitutions (Table 3). Thus, substitution effects of DPA and Cz are beneficial for designing blue-TADF molecules. Meanwhile, for molecules with DPA and Cz substitutions, the ΔE_{ST} of the molecules with DPA (0.45–0.59 eV) and Cz (0.54–0.63 eV) substitutions are higher than that with DMAC (0.05–0.15 eV), PXZ (0.02–0.06 eV) and PTZ (0.01–0.05 eV) substitutions as shown in Fig. 4b. It is worth noting that, there are only triplet states of T_1 for molecules with DMAC, PXZ and PTZ substitutions (Fig. 4c and Fig. S3, ESI†). However, for molecules with DPA and Cz substitutions, the triplet states of T_1 and T_2 could together provide efficient ISC and RISC processes due to the small energy gap between S_1 and T_n (Fig. 4d, e and Fig. S4, ESI†). For *o*-DPA-QL, the energy gap of S_1–T_1 is 0.45 eV, and the energy gap of S_1–T_2 is 0.02eV. As for *o*-Cz-QL, the energy gap of S_1–T_1 is 0.59 eV, and the energy gap of S_1–T_2 is 0.12 eV. Thus, T_2 may also participate in the ISC and RISC processes for molecules with DPA and Cz substitutions.
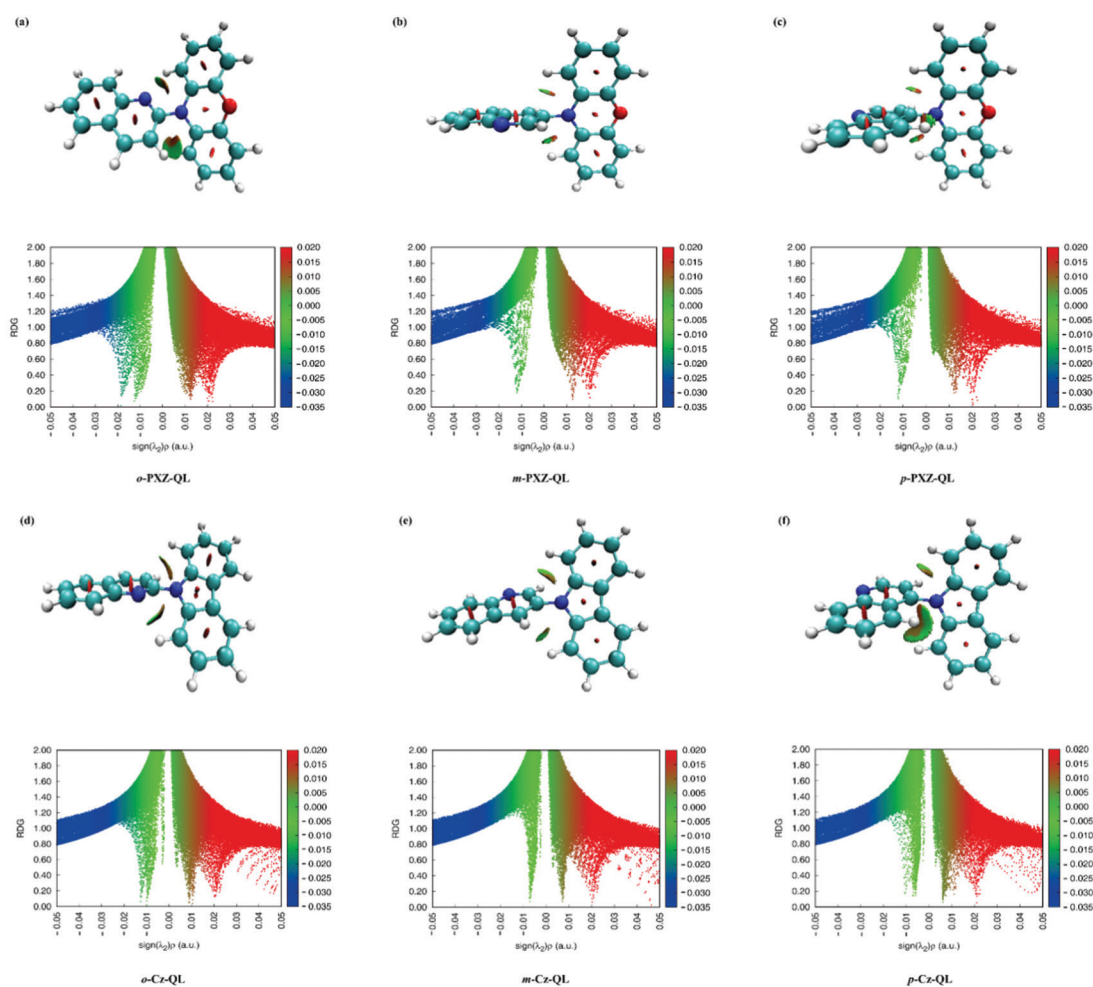

Fig. 3 Reduced density gradient (RDG) isosurface maps (upper) and scatter graphs (lower) of RDG *versus* sign (λ_2) ρ(a.u.) of *o*-PXZ-QL, *m*-PXZ-QL, *p*-PXZ-QL, *o*-Cz-QL, *m*-Cz-QL and *p*-Cz-QL.
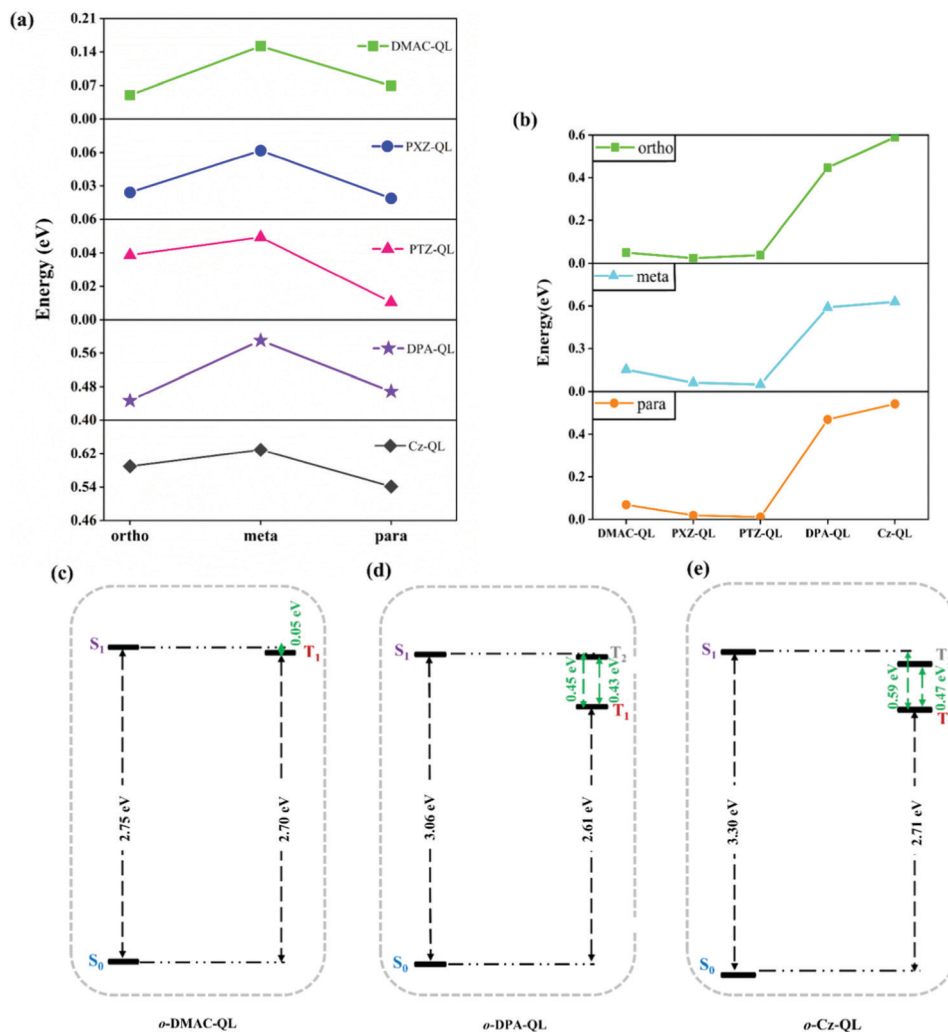
Fig. 4 Comparison of the ΔE_{ST} for molecules with different position substitutions (a) and different donor substitutions (b) of a total of 15 molecules in tetrahydrofuran ($\Delta E_{ST} = S_1 - T_1$). Adiabatic excitation energies for o-DMAC-QL (c), o-DPA-QL (d) and o-Cz-QL (e) in tetrahydrofuran, respectively.

Table 3 Calculated emission wavelength (λ_{em}), adiabatic singlet (S_1) and triplet (T_1) excitation energies ($E_S = S_1 - S_0$, $E_T = T_1 - S_0$) and adiabatic singlet–triplet energy gap (ΔE_{ST}) of all molecules in tetrahydrofuran

	λ_{em} (nm)	E_S (eV)	E_T (eV)	ΔE_{ST} (eV)
o-DMAC-QL	506.24	2.75	2.70	0.05
m-DMAC-QL	495.35	2.69	2.54	0.15
p-DMAC-QL	508.60	2.63	2.56	0.07
o-PXZ-QL	587.76	2.35	2.33	0.02
m-PXZ-QL	571.37	2.40	2.34	0.06
p-PXZ-QL	592.81	2.32	2.30	0.02
o-PTZ-QL	581.31	2.49	2.45	0.04
m-PTZ-QL	569.77	2.50	2.45	0.05
p-PTZ-QL	586.94	2.43	2.42	0.01
o-DPA-QL	469.62	3.06	2.61	0.45
m-DPA-QL	460.74	2.95	2.36	0.59
p-DPA-QL	470.78	2.94	2.47	0.47
o-Cz-QL	408.92	3.30	2.71	0.59
m-Cz-QL	408.24	3.23	2.60	0.63
p-Cz-QL	420.51	3.17	2.63	0.54

To sum up, substitution effects of DPA and Cz are conducive to weaker electron-donating ability and the larger energy gap

between S_1 and S_0, compared with substitution effects of DMAC, PXZ and PTZ. These effects provide prerequisites for blue-TADF molecules. Moreover, T_2 may participate in ISC and RISC processes, which will overcome the hindrance from large ΔE_{ST} and improve the fluorescence efficiency. More evidence is provided in the next section.

3.4 Spin orbital coupling effect

3.4.1 The structure of excited states. The structure of excited states has a great influence on photophysical properties, especially the bond length.[68,69] The bond length between the donor and acceptor of S_1 and T_1 for a total of 15 molecules is listed in Table 4. Results indicate that compared with other positions, substitution effects of o-positions have the most obvious increase in bond length of S_1. However, substitution effects of DPA and Cz reduce the bond length of T_1 significantly. In addition, the bond lengths of T_1 for molecules with different position substitutions among DPA and Cz substitutions are in the order of m-substitutions < p-substitutions < o-substitutions. Fortunately, the distances studied above are

This journal is © The Royal Society of Chemistry 2022

J. Mater. Chem. C, 2022, **10**, 4723–4736 | **4729**

Table 4 Collected bond lengths between the donor and acceptor groups for all studied molecules for the lowest singlet (S_1) and triplet (T_1) excited states

	Bond length/Å	
	S_1	T_1
o-DMAC-QL	1.456	1.427
m-DMAC-QL	1.441	1.408
p-DMAC-QL	1.438	1.415
o-PXZ-QL	1.452	1.447
m-PXZ-QL	1.438	1.418
p-PXZ-QL	1.434	1.428
o-PTZ-QL	1.456	1.451
m-PTZ-QL	1.443	1.438
p-PTZ-QL	1.440	1.439
o-DPA-QL	1.452	1.396
m-DPA-QL	1.432	1.386
p-DPA-QL	1.436	1.395
o-Cz-QL	1.441	1.399
m-Cz-QL	1.422	1.390
p-Cz-QL	1.425	1.398
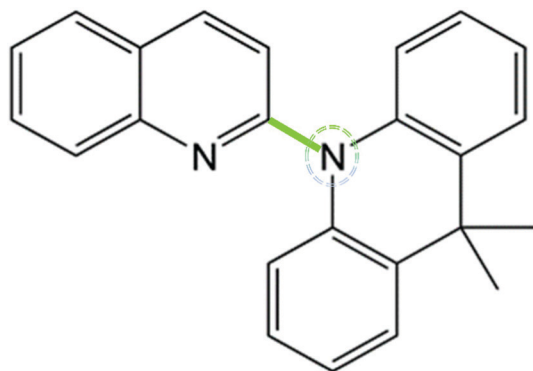
Scheme 1 The bond (green line) between the donor and the acceptor corresponds to the distance from heteroatoms (N) in donor to acceptors.

corresponding to the heteroatoms (N) in the donor to acceptors (as in Scheme 1). As reported by Duan *et al.*,[70] the reducing distance from the heteroatoms in the donor (N) to acceptors can enhance the SOC between singlet and triplet excited states. The specific analyses are as follows.

3.4.2 Natural transition orbitals. The transition properties of the excited state could affect the TADF properties of molecules. Therefore, it is important to analyze the natural transition orbitals of the excited state. The results of 15 molecules studied in present work are shown in Fig. 5 and Fig. S5 (ESI†). According to the proportion of the local-excited (LE) component in transition, transition characters of excited states can be divided into charge-transfer (CT) state (0–40%), hybrid local-excited and charge-transfer (HLCT) state (40–75%), and local-excited (LE) state (75–100%).[71] As shown in Fig. 5b, S_1 and T_1 are classified as the HLCT states, while T_2 is regarded as the LE state for o-DPA-QL, respectively. Results indicate that for the molecules with different position substitutions, the order of LE components for S_1 is: o-substitutions > m-substitutions > p-substitutions. For molecules with DPA and Cz substitutions,

the LE components of them (36–83%) are greater than the molecules with DMAC (18–75%), PXZ (17–70%) and PTZ (20–67%) substitutions, respectively. Furthermore, the difference of LE components (14–46%) between S_1 and T_n of molecules with DPA and Cz substitutions are also greater than molecules with DMAC (1–15%), PXZ (1–16%) and PTZ (5–8%) substitutions (Table S2, ESI†). As the molecules with DMAC, PXZ and PTZ substitutions, a small difference of LE components between S_1 and T_n can bring a small energy gap and a small SOC.[72–75] *Vice versa*, as the molecules with DPA and Cz substitutions, a large difference of LE components between S_1 and T_n could bring a stable triplet state and induce a large SOC value.[35,71,76]

3.4.3 The values of spin-orbital coupling. The processes of ISC and RISC are affected by the SOC as the dominant spin-flipping mechanism.[77,78] Using the Dalton software package, we calculated the SOC values between the singlet and triplet-excited states in the THF solution, and the corresponding data are collected in Table 5. Compared with other positions, the substitution effects of o-positions decrease SOC values most obviously. For the molecules with DPA and Cz substitutions, for both S_1 and T_1, the SOC values (0.30–1.17/0.56–1.56 cm^{-1}) are higher than the molecules with DMAC (0.01–0.09/0.32–0.90 cm^{-1}), PXZ (0.01–0.07/0.40–0.64 cm^{-1}) and PTZ (0.02–0.07/0.04–0.09 cm^{-1}), which are consistent with Section 3.4.1 and 3.4.2. Thus, the SOC values for molecules with DPA and Cz substitutions are substantially higher than the molecules with DMAC, PXZ and PTZ substitutions for S_1 and T_1. In addition, we unexpectedly discovered that for most molecules, the SOC value of the T_n is larger than the S_1, which is undoubtedly beneficial to the RISC process.

In summary, substitution effects of DPA and Cz are beneficial for increasing SOC values, which are good for overcoming hindrances from large ΔE_{ST} and promoting the RISC processes for blue-TADF molecules.

3.5 Decay rates and fluorescence efficiency

Furthermore, in order to study the excited state dynamics in detail, K_r, the non-radiation rate (K_{nr}), the intersystem crossing rate (K_{ISC}) and K_{RISC} between the singlet and triplet states and PL quantum efficiencies for all molecules were calculated employing the methods in Section 2. The corresponding data are gathered in Table 6 and Table S3 (ESI†). The ISC rate and RISC rate can be calculated by the following formulas:

$$K_{ISC}^{cal} = \frac{K_{S_1-T_1}^2 + K_{S_1-T_2}^2}{K_{S_1-T_1} + K_{S_1-T_2}} \quad (11)$$

$$K_{RISC}^{cal} = \frac{K_{T_1-S_1}^2 + K_{T_2-S_1}^2}{K_{T_1-S_1} + K_{T_2-S_1}} \quad (12)$$

Results indicate that the non-radiation rates from S_1 to S_0 (K_{nr}^S) as well as from T_1 to S_0 (K_{nr}^T) of the molecules with p-substitutions are smaller than molecules with o-substitutions and m-substitutions, they are caused by the relatively small reorganization energies between S_1 and S_0 (Table S4, ESI†) and
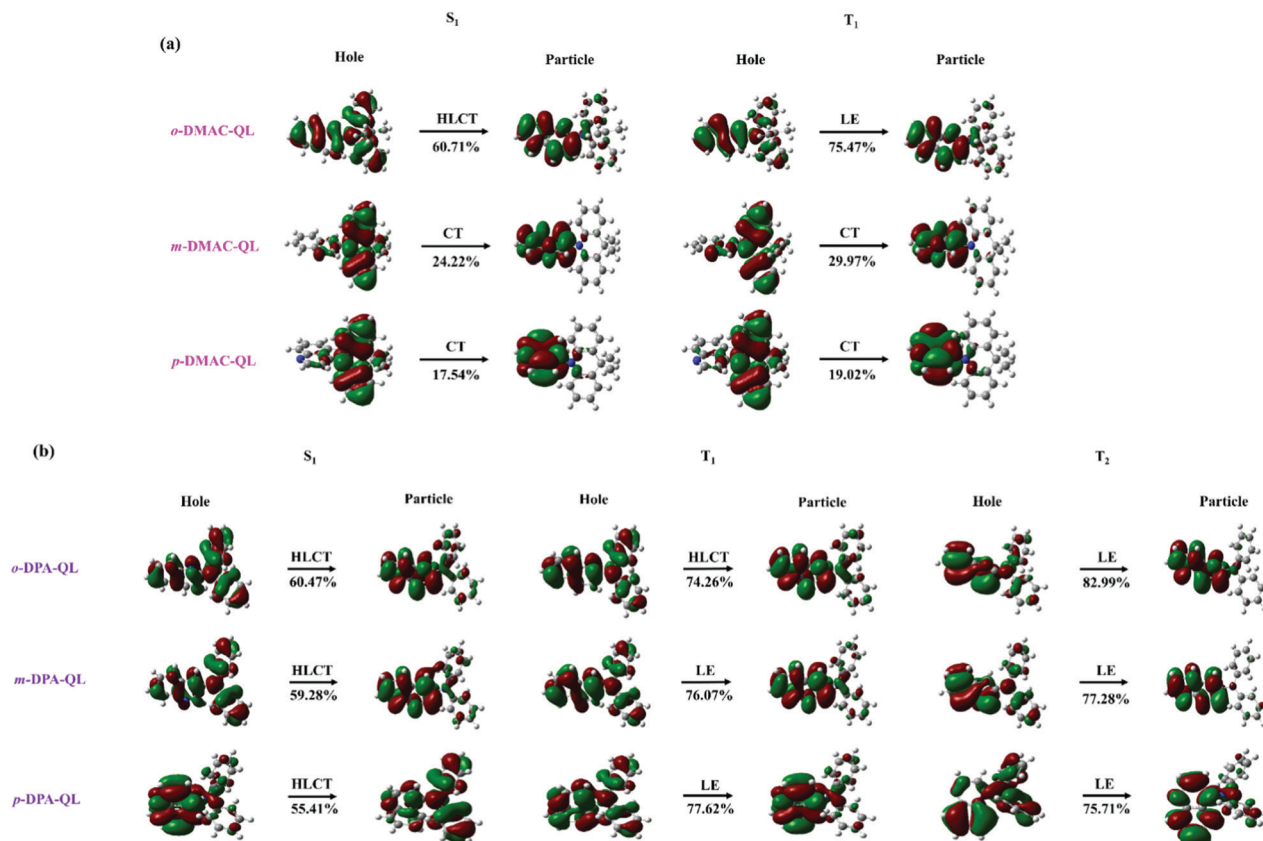
4730 | *J. Mater. Chem. C*, 2022, **10**, 4723–4736

This journal is © The Royal Society of Chemistry 2022

Fig. 5   Natural transition orbitals (NTOs) of the S_1 and T_n states for o-DMAC-QL, m-DMAC-QL, p-DMAC-QL, o-DPA-QL, m-DPA-QL and p-DPA-QL in tetrahydrofuran. The values below the arrows are the LE proportion in excitation.

Table 5   Calculated spin–orbit coupling constants (in cm^{-1}) between the selected singlet and triplet-excited states of all molecules in THF based on the optimized S_1, T_1 and T_2 structures, respectively

	$\langle S_1|\hat{H}_{so}|T_1 \rangle$		$\langle S_1|\hat{H}_{so}|T_2 \rangle$	
	S_1	T_1	S_1	T_2
o-DMAC-QL	0.01	0.32	—	—
m-DMAC-QL	0.09	0.90	—	—
p-DMAC-QL	0.03	0.64	—	—
o-PXZ-QL	0.01	0.54	—	—
m-PXZ-QL	0.07	0.64	—	—
p-PXZ-QL	0.03	0.40	—	—
o-PTZ-QL	0.02	0.04	—	—
m-PTZ-QL	0.07	0.09	—	—
p-PTZ-QL	0.03	0.04	—	—
o-DPA-QL	0.35	1.20	0.99	1.17
m-DPA-QL	0.79	0.92	0.78	1.01
p-DPA-QL	0.71	0.56	0.35	0.26
o-Cz-QL	0.30	0.79	0.96	1.00
m-Cz-QL	1.17	1.56	0.75	0.95
p-Cz-QL	0.74	0.72	0.05	0.05

the smallest values of H_{SO} between T_1 and S_0 (Table S5, ESI†), respectively. Meanwhile, molecules with DPA and Cz substitutions, the radiation rate (K_r^S) from S_1 to S_0 (10^3–10^7 s^{-1}) is higher than the molecules with DMAC (10^4–10^5 s^{-1}), PXZ (10^2–10^3 s^{-1}) and PTZ (10^1–10^4 s^{-1}) substitutions, which is due to their larger transition dipole moments (Table S6, ESI†), corresponding to the Section 3.2.

Moreover, the analyses for holes and electron distributions and heat maps are shown in Fig. S7–S9 (ESI†). The hole is mainly distributed on the donor unit and the electron is localized on the acceptor unit. Well-separated distributions can be found. As for fluorescence efficiency, the data are calculated and shown in Fig. 6. The intersystem crossing efficiency (Φ_{ISC}) of molecules with Cz substitutions (61.11–83.12%) and p-DPA-QL (67.50%) are higher than molecules with DMAC (0–14.99%), PXZ (0–10.12%) and PTZ (0–19.41%) substitutions because of the promoted K_{ISC}^{cal} obviously. However, for o-DPA-QL and m-DPA-QL, the Φ_{ISC} (15.90%/14.33%) is smaller than m-PTZ-QL (19.41%) and m-DMAC-QL (14.99%) respectively, which result from considerable competition between K_r^S ($\sim 10^7$ s^{-1}) and K_{ISC}^{cal} ($\sim 10^7$ s^{-1}). Meanwhile, the reverse intersystem crossing efficiency (Φ_{RISC}) of the molecules with DPA and Cz substitutions are considerable in comparison with DMAC, PXZ and PTZ substitutions except for o-PTZ-QL, which is caused by the comparable K_{RISC} of molecules with these substitutions (Table 6). For o-PTZ-QL, the Φ_{RISC} (0.02%) is much smaller than other molecules because of its large K_{nr}^T. As a consequence, based on the above analyses, 5 promising efficient blue-TADF molecules, namely o-DPA-QL, m-DPA-QL, p-DPA-QL, o-Cz-QL and m-Cz-QL with 8.39%Φ_{PF}/1.59%Φ_{DF}, 22.50%Φ_{PF}/3.76%Φ_{DF}, 5.39%Φ_{PF}/11.19%Φ_{DF}, 8.32%Φ_{PF}/33.25%Φ_{DF} and 7.52%Φ_{PF}/36.98%Φ_{DF}, respectively, are theoretically proposed as good blue TADF candidates. According to Section 3.1, the 5 above molecules have single conformations,

This journal is © The Royal Society of Chemistry 2022

J. Mater. Chem. C, 2022, **10**, 4723–4736 | **4731**

Table 6 Calculated radiative and non-radiative rates as well as the ISC and RISC rates

|	K_{nr}^{S} (S$_1$ → S$_0$) (s^{-1})	K_{r}^{S} (S$_1$ → S$_0$) (s^{-1})	K_{ISC}^{cal} (S$_1$ → T$_n$) (s^{-1})	K_{RISC}^{cal} (T$_n$ → S$_1$) (s^{-1})	K_{r}^{T} (T$_1$ → S$_0$) (s^{-1})	K_{nr}^{T} (T$_1$ → S$_0$) (s^{-1})	Φ_{ISC} (%)	Φ_{RISC} (%)	Φ_{PF} (%)	Φ_{DF} (%)
o-DMAC-QL	5.56×10^{11}	4.97×10^{4}	1.75×10^{4}	8.84×10^{6}	9.50	1.26×10^{3}	0.00	99.99	0.00	0.00
m-DMAC-QL	1.87×10^{7}	1.97×10^{5}	3.34×10^{6}	6.09×10^{5}	1.77	8.82×10^{2}	14.99	99.85	0.89	0.16
p-DMAC-QL	3.17×10^{6}	1.11×10^{4}	2.88×10^{5}	2.18×10^{7}	1.43	3.59×10^{1}	8.31	100.00	0.32	0.03
o-PXZ-QL	6.81×10^{11}	5.23×10^{2}	6.08×10^{4}	3.30×10^{8}	1.64	1.16×10^{6}	0.00	99.65	0.00	0.00
m-PXZ-QL	2.50×10^{7}	5.14×10^{3}	2.44×10^{6}	2.47×10^{7}	1.86	2.20×10^{2}	8.91	100.00	0.02	0.00
p-PXZ-QL	4.77×10^{6}	3.72×10^{4}	5.38×10^{5}	1.23×10^{8}	1.01	3.86×10^{1}	10.12	100.00	0.05	0.01
o-PTZ-QL	1.53×10^{11}	3.12×10^{1}	8.52×10^{4}	1.04×10^{5}	0.06	6.16×10^{8}	0.00	0.02	0.00	0.00
m-PTZ-QL	2.26×10^{7}	3.26×10^{4}	5.45×10^{6}	2.54×10^{6}	3.13	4.82×10^{4}	19.41	98.14	0.12	0.02
p-PTZ-QL	7.46×10^{6}	2.50×10^{3}	7.85×10^{5}	4.48×10^{6}	1.11	4.06×10^{4}	9.51	99.10	0.03	0.00
o-DPA-QL	1.24×10^{8}	1.37×10^{7}	2.61×10^{7}	1.07×10^{7}	1.65	1.43×10^{2}	15.90	100.00	8.39	1.59
m-DPA-QL	7.31×10^{7}	2.60×10^{7}	1.66×10^{7}	3.18×10^{8}	0.41	2.90×10^{2}	14.33	100.00	22.50	3.76
p-DPA-QL	6.12×10^{7}	1.22×10^{7}	1.52×10^{8}	1.64×10^{7}	0.56	3.00×10^{1}	67.50	100.00	5.39	11.19
o-Cz-QL	4.10×10^{7}	2.93×10^{7}	2.81×10^{8}	8.14×10^{5}	1.61	2.27×10^{2}	80.01	99.97	8.32	33.25
m-Cz-QL	2.82×10^{7}	2.26×10^{7}	2.50×10^{8}	1.89×10^{7}	0.71	1.10×10^{3}	83.12	99.99	7.52	36.98
p-Cz-QL	2.32×10^{7}	5.96×10^{3}	3.65×10^{7}	2.11×10^{5}	0.63	7.14×10^{1}	61.11	99.97	0.01	0.02
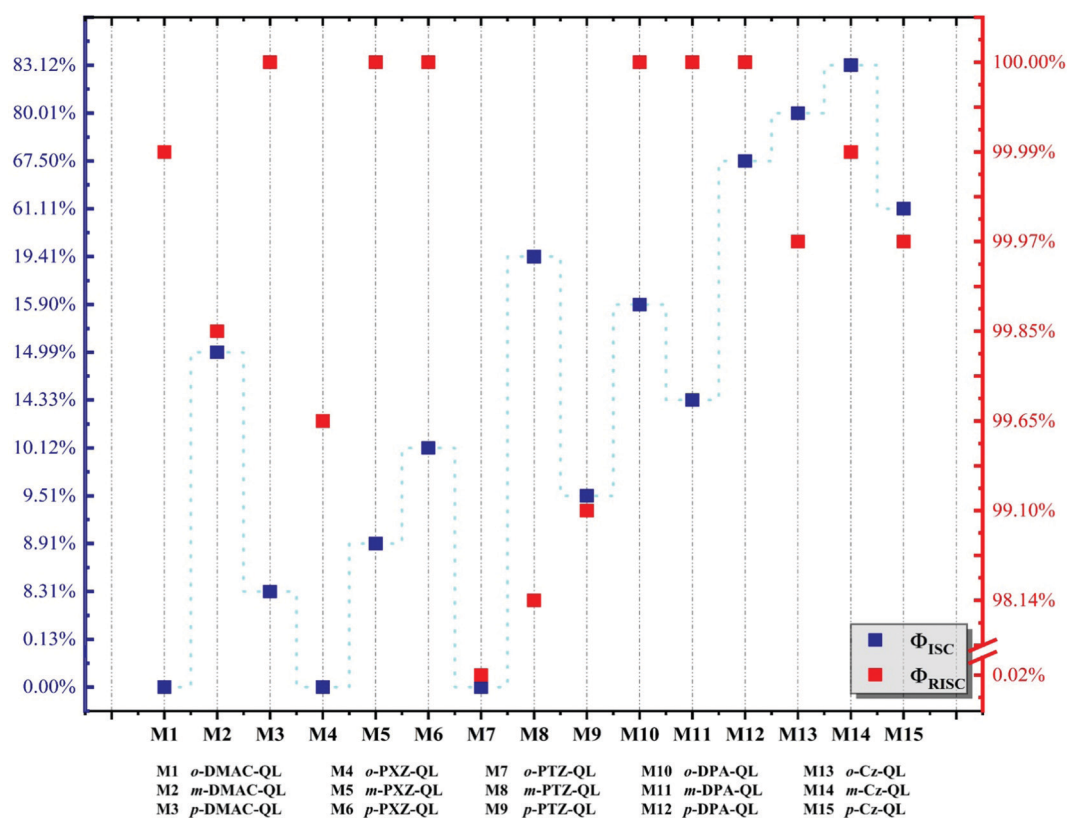
Fig. 6 Calculated the intersystem crossing efficiency (blue square) and reverse intersystem crossing efficiency (red square) of a total of 15 molecules, respectively.

which are beneficial for achieving better performance in real applications because there are no other conformations that may give rise to adverse effects.

4. Conclusions

In summary, the photophysical properties of a total of 15 TADF molecules were theoretically studied using DFT and TD-DFT coupled with the TVCF method. Substitution effects of different donors (DMAC, PXZ, PTZ, DPA and Cz) and different positions (ortho, meta and para) on TADF features were analyzed in detail. The conformational isomerization, intramolecular interactions, energy gaps, SOCs, and fluorescence efficiencies were systemically investigated. Results indicate that substitution effects of DPA and Cz increase the energy gap between S$_1$ and S$_0$. In addition, the substitution effects bring weak electron-donating ability. These factors provide prerequisites for blue-TADF

4732 | *J. Mater. Chem. C*, 2022, **10**, 4723–4736

This journal is © The Royal Society of Chemistry 2022

molecules. However, the substitution effects bring the large ΔE_{ST} to molecules with *m*-substitutions, which are a disadvantage for designing blue-TADF molecules. Fortunately, the large SOC value between S_1 and T_n will overcome hindrances from large ΔE_{ST}. Meanwhile, due to larger K_{ISC} and K_r, molecules with DPA and Cz substitutions possess larger Φ_{ISC}. Due to comparable K_{RISC}, these molecules possess considerable Φ_{RISC}. Furthermore, five new efficient blue-TADF molecules with promising applications are theoretically proposed. Our work provides reasonable explanations for experimental results, substitution effects of different donors and different positions on TADF properties are highlighted and structure–property relationships are illustrated, which are conducive to understanding the inner regulatory mechanisms of D–A typed TADF molecules.

Conflicts of interest

There are no conflicts of interest to declare.

Acknowledgements

References

1   A. Endo, M. Ogasawara, A. Takahashi, D. Yokoyama, Y. Kato and C. Adachi, Thermally activated delayed fluorescence from Sn^{4+}–porphyrin complexes and their application to organic light emitting diodes—A novel mechanism for electroluminescence, *Adv. Mater.*, 2009, **21**(47), 4802–4806.

2   H. Uoyama, K. Goushi, K. Shizu, H. Nomura and C. Adachi, Highly efficient organic light-emitting diodes from delayed fluorescence, *Nature*, 2012, **492**(7428), 234–238.

3   B. Huang, W. C. Chen, Z. Li, J. Zhang, W. Zhao, Y. Feng, B. Z. Tang and C. S. Lee, Manipulation of molecular aggregation states to realize polymorphism, AIE, MCL, and TADF in a single molecule, *Angew. Chem.*, 2018, **130**(38), 12653–12657.

4   D. Liu, J. Y. Wei, W. W. Tian, W. Jiang, Y. M. Sun, Z. Zhao and B. Z. Tang, Endowing TADF luminophors with AIE properties through adjusting flexible dendrons for highly efficient solution-processed nondoped OLEDs, *Chem. Sci.*, 2020, **11**(27), 7194–7203.

5   D. Wei, F. Ni, Z. Wu, Z. Zhu, Y. Zou, K. Zheng, Z. Chen, D. Ma and C. Yang, Designing dual emitting cores for highly efficient thermally activated delayed fluorescent emitters, *J. Mater. Chem. C*, 2018, **6**(43), 11615–11621.

6   J. Zhang, Y. Wei and H. Xu, High-power-efficiency thermally activated delayed fluorescence white organic light-emitting diodes based on asymmetrical host engineering, *Nano Energy*, 2021, **83**, 105746.

7   W. Wei, Z. Yang, X. Chen, T. Liu, Z. Mao, J. Zhao and Z. Chi, Modulation of π-linkers in asymmetric thermally activated delayed fluorescence molecules enabling high performance OLEDs, *J. Mater. Chem. C*, 2020, **8**(11), 3663–3668.

8   M. Ouyang, L. Xing, Q. Chen, H. Huang, M. Zhu, K. Hu, Y. Liu, W.-C. Chen, Y. Huo and C. Yang, Highly efficient thermally activated delayed fluorescence emitters enabled by double charge transfer pathways via ortho-linked tri-arylboron/carbazole hybrids, *J. Mater. Chem. C*, 2021, **9**(5), 1678–1684.

9   X. Zhan, Z. Wu, Y. Gong, J. Tu, Y. Xie, Q. Peng, D. Ma, Q. Li and Z. Li, Utilizing Electroplex Emission to Achieve External Quantum Efficiency up to 18.1% in Nondoped Blue OLED, *Research*, 2020, **2020**, 1–13.

10 D. Zhang, X. Song, A. J. Gillett, B. H. Drummond, S. T. Jones, G. Li, H. He, M. Cai, D. Credgington and L. Duan, Efficient and Stable Deep-Blue Fluorescent Organic Light-Emitting Diodes Employing a Sensitizer with Fast Triplet Upconversion, *Adv. Mater.*, 2020, **32**(19), 1908355.

11 O. Bezvikonnyi, D. Gudeika, D. Volyniuk, V. Mimaite, B. R. Sebastine and J. V. Grazulevicius, Effect of donor substituents on thermally activated delayed fluorescence of diphenylsulfone derivatives, *J. Lumin.*, 2019, **206**, 250–259.

12 L. Gan, Z. Xu, Z. Wang, B. Li, W. Li, X. Cai, K. Liu, Q. Liang and S. J. Su, Utilizing a spiro TADF moiety as a functional electron donor in TADF molecular design toward efficient "multichannel" reverse intersystem crossing, *Adv. Funct. Mater.*, 2019, **29**(20), 1808088.

13 J.-L. He, F.-C. Kong, B. Sun, X.-J. Wang, Q.-S. Tian, J. Fan and L.-S. Liao, Highly Efficient Deep-Red TADF Organic Light-Emitting Diodes via Increasing the Acceptor Strength of Fused Polycyclic Aromatics, *Chem. Eng. J.*, 2021, 130470.

14 Y. Kitamoto, T. Namikawa, T. Suzuki, Y. Miyata, H. Kita, T. Sato and S. Oi, Design and synthesis of efficient blue thermally activated delayed fluorescence molecules bearing triarylborane and 10, 10-dimethyl-5, 10-dihydrophenazasiline moieties, *Tetrahedron Lett.*, 2016, **57**(44), 4914–4917.

15 J. Leng, Z. Zhang, Y. Zhang, J. Sun and H. Ma, Excited state properties of two unusual thermally activated delayed fluorescence molecules: A theoretical investigation, *J. Lumin.*, 2018, **204**, 312–318.

16 L. Liu, Q. Wei, Y. Cheng, H. Ma, S. Xiong and X. Zhang, Theoretical studies on full-color thermally activated delayed fluorescence molecules, *J. Mater. Chem. C*, 2020, **8**(17), 5839–5846.

17 Y. Qi, J. Zhao, X. Wang, J. Yu and Z. Chi, High-efficiency phosphorescent organic light-emitting devices with low efficiency roll-off using a thermally activated delayed fluorescence material as host, *Org. Electron.*, 2016, **36**, 185–191.

18 Y. Tan, B. Rui, J. Li, Z. Zhao, Z. Liu, Z. Bian and C. Huang, Blue thermally activated delayed fluorescence emitters based on a constructing strategy with diversed donors and

oxadiazole acceptor and their efficient electroluminescent devices, *Opt. Mater.*, 2019, **94**, 103–112.

19 C. Wu, Q. Guo, W. Ma, X. Li, P. Qiu, J. Hu, Q. Wang, J. Chen and D. Ma, Hybrid host materials for highly efficient electrophosphorescence and thermally activated delayed fluorescence independent of the linkage mode, *Phys. Chem. Chem. Phys.*, 2017, **19**(7), 5177–5184.

20 H. Xu, T. Yang, F. Wang, J. Zhang, X. Zhang, H. Wang and B. Xu, Thermally activated delayed fluorescence of copper(I) complexes using *N,N'*-heteroaromatic of 2-(5-phenyl-1, 2, 3-triazole) pyridine as ligand, *J. Lumin.*, 2019, **205**, 82–86.

21 Z. Zhao, C. Y. Chan, S. Chen, C. Deng, J. W. Lam, C. K. Jim, Y. Hong, P. Lu, Z. Chang and X. Chen, Using tetraphenyl-ethene and carbazole to create efficient luminophores with aggregation-induced emission, high thermal stability, and good hole-transporting property, *J. Mater. Chem.*, 2012, **22**(10), 4527–4534.

22 Z. Zhao, C. Deng, S. Chen, J. W. Lam, W. Qin, P. Lu, Z. Wang, H. S. Kwok, Y. Ma and H. Qiu, Full emission color tuning in luminogens constructed from tetraphenylethene, benzo-2, 1, 3-thiadiazole and thiophene building blocks, *Chem. Commun.*, 2011, **47**(31), 8847–8849.

23 W. Zhiqiang, C. Jialin, Z. Ming, Z. Caijun and J. Baoming, A Novel Yellow Thermally Activated Delayed Fluorescence Emitter For Highly Efficient Organic Light-Emitting Diodes, *Acta Chim. Sin.*, 2019, **77**(3), 263–268.

24 Y. J. Cho, S. K. Jeon, B. D. Chin, E. Yu and J. Y. Lee, The design of dual emitting cores for green thermally activated delayed fluorescent materials, *Angew. Chem., Int. Ed.*, 2015, **54**(17), 5201–5204.

25 S. Hu, J. Zeng, X. Zhu, J. Guo, S. Chen, Z. Zhao and B. Z. Tang, Universal bipolar host materials for blue, green, and red phosphorescent OLEDs with excellent efficiencies and small-efficiency roll-off, *ACS Appl. Mater. Interfaces*, 2019, **11**(30), 27134–27144.

26 S. Wang, Y. Miao, X. Yan, K. Ye and Y. Wang, A dibenzo[*a,c*]phenazine-11, 12-dicarbonitrile (DBPzDCN) acceptor based thermally activated delayed fluorescent compound for efficient near-infrared electroluminescent devices, *J. Mater. Chem. C*, 2018, **6**(25), 6698–6704.

27 S. Wang, X. Yan, Z. Cheng, H. Zhang, Y. Liu and Y. Wang, Highly efficient near-infrared delayed fluorescence organic light emitting diodes using a phenanthrene-based charge-transfer compound, *Angew. Chem., Int. Ed.*, 2015, **54**(44), 13068–13072.

28 Y. Yuan, Y. Hu, Y. X. Zhang, J. D. Lin, Y. K. Wang, Z. Q. Jiang, L. S. Liao and S. T. Lee, Over 10% EQE Near-Infrared Electroluminescence Based on a Thermally Activated Delayed Fluorescence Emitter, *Adv. Funct. Mater.*, 2017, **27**(26), 1700986.

29 K. Goushi, K. Yoshida, K. Sato and C. Adachi, Organic light-emitting diodes employing efficient reverse intersystem crossing for triplet-to-singlet state conversion, *Nat. Photonics*, 2012, **6**(4), 253–258.

30 J. Huang, N. Sun, J. Yang, R. Tang, Q. Li, D. Ma and Z. Li, Blue Aggregation-Induced Emission Luminogens: High External

Quantum Efficiencies Up to 3.99% in LED Device, and Restriction of the Conjugation Length through Rational Molecular Design, *Adv. Funct. Mater.*, 2014, **24**(48), 7645–7654.

31 M. Zhu and C. Yang, Blue fluorescent emitters: design tactics and applications in organic light-emitting diodes, *Chem. Soc. Rev.*, 2013, **42**(12), 4963–4976.

32 W. Li, X. Cai, B. Li, L. Gan, Y. He, K. Liu, D. Chen, Y. C. Wu and S. J. Su, Adamantane-Substituted Acridine Donor for Blue Dual Fluorescence and Efficient Organic Light-Emitting Diodes, *Angew. Chem.*, 2019, **131**(2), 592–596.

33 K. Shizu, H. Noda, H. Tanaka, M. Taneda, M. Uejima, T. Sato, K. Tanaka, H. Kaji and C. Adachi, Highly efficient blue electroluminescence using delayed-fluorescence emitters with large overlap density between luminescent and ground states, *J. Phys. Chem. C*, 2015, **119**(47), 26283–26289.

34 Y.-F. Shen, M. Li, W.-L. Zhao, Y.-F. Wang, H.-Y. Lu and C.-F. Chen, Quinoline-based TADF emitters exhibiting aggregation-induced emission for efficient non-doped organic light-emitting diodes, *Mater. Chem. Front.*, 2021, **5**(2), 834–842.

35 M. K. Etherington, F. Franchello, J. Gibson, T. Northey, J. Santos, J. S. Ward, H. F. Higginbotham, P. Data, A. Kurowska and P. L. Dos, Santos, Regio-and conformational isomerization critical to design of efficient thermally-activated delayed fluorescence emitters, *Nat. Commun.*, 2017, **8**(1), 1–11.

36 X. K. Liu, Z. Chen, J. Qing, W. J. Zhang, B. Wu, H. L. Tam, F. Zhu, X. H. Zhang and C. S. Lee, Remanagement of singlet and triplet excitons in single-emissive-layer hybrid white organic light-emitting devices using thermally activated delayed fluorescent blue exciplex, *Adv. Mater.*, 2015, **27**(44), 7079–7085.

37 M. J. Frisch, G. W. Trucks, H. B. Schlegel, G. E. Scuseria, M. A. Robb, J. R. Cheeseman, G. Scalmani, V. Barone, G. A. Petersson, H. Nakatsuji, X. Li, M. Caricato, A. V. Marenich, J. Bloino, B. G. Janesko, R. Gomperts, B. Mennucci, H. P. Hratchian, J. V. Ortiz, A. F. Izmaylov, J. L. Sonnenberg, D. Williams-Young, F. Ding, F. Lipparini, F. Egidi, J. Goings, B. Peng, A. Petrone, T. Henderson, D. Ranasinghe, V. G. Zakrzewski, J. Gao, N. Rega, G. Zheng, W. Liang, M. Hada, M. Ehara, K. Toyota, R. Fukuda, J. Hasegawa, M. Ishida, T. Nakajima, Y. Honda, O. Kitao, H. Nakai, T. Vreven, K. Throssell, J. A. Montgomery, Jr., J. E. Peralta, F. Ogliaro, M. J. Bearpark, J. J. Heyd, E. N. Brothers, K. N. Kudin, V. N. Staroverov, T. A. Keith, R. Kobayashi, J. Normand, K. Raghavachari, A. P. Rendell, J. C. Burant, S. S. Iyengar, J. Tomasi, M. Cossi, J. M. Millam, M. Klene, C. Adamo, R. Cammi, J. W. Ochterski, R. L. Martin, K. Morokuma, O. Farkas, J. B. Foresman and D. J. Fox, *Gaussian, Inc.*, Wallingford CT, 2016.

38 J.-Z. Fan, S. Qiu, L.-L. Lin and C.-K. Wang, First-principles investigation on triazine based thermally activated delayed fluorescence emitters, *Chin. J. Chem. Phys.*, 2016, **29**(3), 291.

39 J. Tomasi, B. Mennucci and R. Cammi, Quantum mechanical continuum solvation models, *Chem. Rev.*, 2005, **105**(8), 2999–3094.

4734 | *J. Mater. Chem. C*, 2022, **10**, 4723–4736

This journal is © The Royal Society of Chemistry 2022

40 J.-Z. Fan, L.-L. Lin and C.-K. Wang, Decreasing the singlet–triplet gap for thermally activated delayed fluorescence molecules by structural modification on the donor fragment: First-principles study, *Chem. Phys. Lett.*, 2016, **652**, 16–21.

41 W.-M. Hoe, A. J. Cohen and N. C. Handy, Assessment of a new local exchange functional OPTX, *Chem. Phys. Lett.*, 2001, **341**(3-4), 319–328.

42 P. Stephens, C. Chabalowski, F. Devlin and K. Jalkanen, Ab initio calculation of vibrational circular dichroism spectra using large basis set MP2 force fields, *Chem. Phys. Lett.*, 1994, **225**(1-3), 247–257.

43 C. Adamo and V. Barone, Toward reliable density functional methods without adjustable parameters: The PBE0 model, *J. Chem. Phys.*, 1999, **110**(13), 6158–6170.

44 A. D. Boese and J. M. Martin, Development of density functionals for thermochemical kinetics, *J. Chem. Phys.*, 2004, **121**(8), 3405–3416.

45 Y. Tao, K. Yuan, T. Chen, P. Xu, H. Li, R. Chen, C. Zheng, L. Zhang and W. Huang, Thermally activated delayed fluorescence materials towards the breakthrough of organoelectronics, *Adv. Mater.*, 2014, **26**(47), 7931–7958.

46 K. Aidas, C. Angeli, K. L. Bak, V. Bakken, R. Bast, L. Boman, O. Christiansen, R. Cimiraglia, S. Coriani and P. Dahle, The D alton quantum chemistry program system, *Wiley Interdiscip. Rev.: Comput. Mol. Sci.*, 2014, **4**(3), 269–284.

47 Dalton. a Molecular Electronic Structure Program. Release Dalton2013, 2014, available from: http://daltonprogram.org.

48 Y. Niu, W. Li, Q. Peng, H. Geng, Y. Yi, L. Wang, G. Nan, D. Wang and Z. Shuai, MOlecular MAterials Property Prediction Package (MOMAP) 1.0: a software package for predicting the luminescent properties and mobility of organic functional materials, *Mol. Phys.*, 2018, **116**(7–8), 1078–1090.

49 J. Fan, L. Lin and C.-K. Wang, Excited state properties of non-doped thermally activated delayed fluorescence emitters with aggregation-induced emission: a QM/MM study, *J. Mater. Chem. C*, 2017, **5**(33), 8390–8399.

50 L. Lin, Z. Wang, J. Fan and C. Wang, Theoretical insights on the electroluminescent mechanism of thermally activated delayed fluorescence emitters, *Org. Electron.*, 2017, **41**, 17–25.

51 Q. Ou, Q. Peng and Z. Shuai, Toward Quantitative Prediction of Fluorescence Quantum Efficiency by Combining Direct Vibrational Conversion and Surface Crossing: BODIPYs as an Example, *J. Phys. Chem. Lett.*, 2020, **11**(18), 7790–7797.

52 Q. Peng, D. Fan, R. Duan, Y. Yi, Y. Niu, D. Wang and Z. Shuai, Theoretical study of conversion and decay processes of excited triplet and singlet states in a thermally activated delayed fluorescence molecule, *J. Phys. Chem. C*, 2017, **121**(25), 13448–13456.

53 J. R. Reimers, A practical method for the use of curvilinear coordinates in calculations of normal-mode-projected displacements and Duschinsky rotation matrices for large molecules, *J. Chem. Phys.*, 2001, **115**(20), 9103–9109.

54 Z. Shuai and Q. Peng, Organic light-emitting diodes: theoretical understanding of highly efficient materials and development of computational methodology, *Natl. Sci. Rev.*, 2017, **4**(2), 224–239.

55 Y. Wang, J. Ren and Z. Shuai, Evaluating the anharmonicity contributions to the molecular excited state internal conversion rates with finite temperature TD-DMRG, *J. Chem. Phys.*, 2021, **154**(21), 214109.

56 T. Lu and F. Chen, Multiwfn: a multifunctional wavefunction analyzer, *J. Comput. Chem.*, 2012, **33**(5), 580–592.

57 M. Okazaki, Y. Takeda, P. Data, P. Pander, H. Higginbotham, A. P. Monkman and S. Minakata, Thermally activated delayed fluorescent phenothiazine–dibenzo[*a,j*]phenazine–phenothiazine triads exhibiting tricolor-changing mechanochromic luminescence, *Chem. Sci.*, 2017, **8**(4), 2677–2686.

58 H. Tanaka, K. Shizu, H. Nakanotani and C. Adachi, Dual intramolecular charge-transfer fluorescence derived from a phenothiazine-triphenyltriazine derivative, *J. Phys. Chem. C*, 2014, **118**(29), 15985–15994.

59 Y. Kitamoto, T. Namikawa, D. Ikemizu, Y. Miyata, T. Suzuki, H. Kita, T. Sato and S. Oi, Light blue and green thermally activated delayed fluorescence from 10*H*-phenoxaborin-derivatives and their application to organic light-emitting diodes, *J. Mater. Chem. C*, 2015, **3**(35), 9122–9130.

60 K. Wang, C. J. Zheng, W. Liu, K. Liang, Y. Z. Shi, S. L. Tao, C. S. Lee, X. M. Ou and X. H. Zhang, Avoiding energy loss on TADF emitters: controlling the dual conformations of D–A structure molecules based on the pseudoplanar segments, *Adv. Mater.*, 2017, **29**(47), 1701476.

61 T.-L. Wu, S.-Y. Liao, P.-Y. Huang, Z.-S. Hong, M.-P. Huang, C.-C. Lin, M.-J. Cheng and C.-H. Cheng, Exciplex organic light-emitting diodes with nearly 20% external quantum efficiency: effect of intermolecular steric hindrance between the donor and acceptor pair, *ACS Appl. Mater. Interfaces*, 2019, **11**(21), 19294–19300.

62 J. Lou, X. Tang, H. Zhang, W. Guan and C. Lu, Chemiluminescence Resonance Energy Transfer Efficiency and Donor–Acceptor Distance: from Qualitative to Quantitative, *Angew. Chem., Int. Ed.*, 2021, **60**, 2–9.

63 J. Jiang, D. Hu, M. Hanif, X. Li, S. Su, Z. Xie, L. Liu, S. Zhang, B. Yang and Y. Ma, Twist angle and rotation freedom effects on luminescent donor–acceptor materials: crystal structures, photophysical properties, and OLED application, *Adv. Opt. Mater.*, 2016, **4**(12), 2109–2118.

64 T. Lu and F. Chen, Revealing the nature of intermolecular interaction and configurational preference of the nonpolar molecular dimers (H2)2, (N2)2, and (H2)(N2), *J. Mol. Model.*, 2013, **19**(12), 5387–5395.

65 T. Chen, L. Zheng, J. Yuan, Z. An, R. Chen, Y. Tao, H. Li, X. Xie and W. Huang, Understanding the control of singlet-triplet splitting for organic exciton manipulating: a combined theoretical and experimental approach, *Sci. Rep.*, 2015, **5**(1), 1–11.

66 S. Huang, Q. Zhang, Y. Shiota, T. Nakagawa, K. Kuwabara, K. Yoshizawa and C. Adachi, Computational prediction for singlet-and triplet-transition energies of charge-transfer compounds, *J. Chem. Theory Comput.*, 2013, **9**(9), 3872–3877.

67 W. Che, Y. Xie and Z. Li, Structural Design of Blue-to-Red Thermally-Activated Delayed Fluorescence Molecules by Adjusting the Strength between Donor and Acceptor, *Asian J. Org. Chem.*, 2020, **9**(9), 1262–1276.

This journal is © The Royal Society of Chemistry 2022

J. Mater. Chem. C, 2022, **10**, 4723–4736 | **4735**

68 S. Xu, Q. Yang, Y. Wan, R. Chen, S. Wang, Y. Si, B. Yang, D. Liu, C. Zheng and W. Huang, Predicting intersystem crossing efficiencies of organic molecules for efficient thermally activated delayed fluorescence, *J. Mater. Chem. C*, 2019, **7**(31), 9523–9530.

69 M. Yang, I. S. Park, Y. Miyashita, K. Tanaka and T. Yasuda, Mechanochromic Delayed Fluorescence Switching in Propeller-Shaped Carbazole–Isophthalonitrile Luminogens with Stimuli-Responsive Intramolecular Charge-Transfer Excited States, *Angew. Chem., Int. Ed.*, 2020, **59**(33), 13955–13961.

70 M. Cai, M. Auffray, D. Zhang, Y. Zhang, R. Nagata, Z. Lin, X. Tang, C.-Y. Chan, Y.-T. Lee and T. Huang, Enhancing spin-orbital coupling in deep-blue/blue TADF emitters by minimizing the distance from the heteroatoms in donors to acceptors, *Chem. Eng. J.*, 2021, **420**, 127591.

71 R. Chen, Y. Tang, Y. Wan, T. Chen, C. Zheng, Y. Qi, Y. Cheng and W. Huang, Promoting singlet/triplet exciton transformation in organic optoelectronic molecules: role of excited state transition configuration, *Sci. Rep.*, 2017, **7**(1), 1–11.

72 M. K. Etherington, J. Gibson, H. F. Higginbotham, T. J. Penfold and A. P. Monkman, Revealing the spin–vibronic coupling mechanism of thermally activated delayed fluorescence, *Nat. Commun.*, 2016, **7**(1), 1–7.

73 J. Gibson, A. P. Monkman and T. J. Penfold, The importance of vibronic coupling for efficient reverse intersystem crossing in thermally activated delayed fluorescence molecules, *Chem. Phys. Chem.*, 2016, **17**(19), 2956.

74 Y. Ma, K. Zhang, Y. Zhang, Y. Song, L. Lin, C.-K. Wang and J. Fan, Effects of Secondary Acceptors on Excited-State Properties of Sky-Blue Thermally Activated Delayed Fluorescence Molecules: Luminescence Mechanism and Molecular Design, *J. Phys. Chem. A*, 2020, **125**(1), 175–186.

75 R. S. Nobuyasu, J. S. Ward, J. Gibson, B. A. Laidlaw, Z. Ren, P. Data, A. S. Batsanov, T. J. Penfold, M. R. Bryce and F. B. Dias, The influence of molecular geometry on the efficiency of thermally activated delayed fluorescence, *J. Mater. Chem. C*, 2019, **7**(22), 6672–6684.

76 C. M. Marian, Mechanism of the triplet-to-singlet upconversion in the assistant dopant ACRXTN, *J. Phys. Chem. C*, 2016, **120**(7), 3715–3721.

77 J. Gibson and T. Penfold, Nonadiabatic coupling reduces the activation energy in thermally activated delayed fluorescence, *Phys. Chem. Chem. Phys.*, 2017, **19**(12), 8428–8434.

78 M. Y. Wong and E. Zysman-Colman, Purely organic thermally activated delayed fluorescence materials for organic light-emitting diodes, *Adv. Mater.*, 2017, **29**(22), 1605444.